ACS OMEGA

http://pubs.acs.org/journal/acsodf

Article

Probing Liquid–Liquid Phase Separation in Secondary Organic Aerosol Mimicking Solutions Using Articulated Straws

Emmaline R. Longnecker, Lucy Metz, Rebecca S. Miller, and Andrew E. Berke*

Cite This: *ACS Omega* 2021, 6, 33436–33442

Read Online

ACCESS | Metrics & More | Article Recommendations | Supporting Information

ABSTRACT: The presence or absence of liquid–liquid phase separation (LLPS) in aerosol particles containing oxidized organic species and inorganic salts affects particle morphology and influences uptake into, diffusion through, and reactivity within those particles. We report here an accessible method, similar to ice core analyses, using solutions that are relevant for both aerosol chemical systems and aqueous two-phase extraction systems and contain ammonium sulfate and one of eight alcohols (methanol, ethanol, 1-propanol, 2-propanol, 2-butaonol, 3-methyl-2-butanol, 1,2-propanediol, or 1,3-propanediol) frozen in articulated (bendable) straws to probe LLPS. For alcohols with negative octanol–water partitioning coefficient (K_{OW}) values and O/C ratios ≥0.5, no LLPS occurs, while for alcohols with positive K_{OW} values and O/C ratios ≤0.33, phase separation always occurs, both findings consistent with observations using different experimental techniques. When a third species, glyoxal, is added, the glyoxal stays in the aqueous phase, regardless of whether LLPS occurs. When phase separation occurs, the glyoxal forms a strong intermolecular interaction with the sulfate ion, red-shifting the $\nu_3(SO_4^{2-})$ peak by 15 cm^{-1}. These results provide evidence of chemical interactions within phase-separated systems that have implications for understanding chemical reactivity within those, and related, systems.

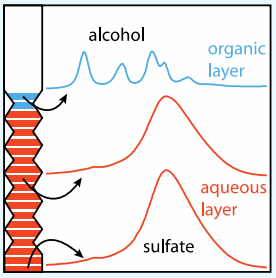

INTRODUCTION

Aerosol particles include substantial organic and inorganic fractions,[1] and this ever-changing internal chemical mixture frequently leads to liquid–liquid phase separation (LLPS). Morphology changes brought on by the onset or loss of LLPS affect partitioning to, diffusion through, and reactivity within a particle.[2−4] LLPS can also alter a particle's optical properties and ability to act as a cloud condensation nucleator.[5] Understanding the physical and chemical changes that aerosol particles undergo as they age and their associated morphologies is important for our ability to better model the climate.[6]

A relatively recent body of both aerosol[7−20] and aqueous, two-phase extraction (ATPE)[21−23] literature has explored LLPS in mixed organic/inorganic systems. Among the variables found to affect the formation of LLPS on the particle scale are chemical composition and relative humidity. Other related studies use particle imaging techniques such as optical tweezers[16] or cryo-TEM[17] to probe bulk structure in particles and droplets.[24] While bulk analyses offer an overview of a particle, probing the boundary between phases or intraparticle organization requires zooming in on the internal composition. The options for investigating these structures and relationships are more limited, though important work has been done using surface-enhanced[18] and confocal[19,20] Raman. In an example of the latter, Wu et al.[19] probed different spatial regions of glutaric acid/magnesium sulfate droplets and found a clear LLPS at high relative humidity with an organic shell and salt-rich core. Song et al.[9−11,25] have also found that when LLPS occurs for aqueous-based particles containing organic and inorganic components, the inner layer is predominantly water-rich. We report here a simple method that, while lacking the micrometer vertical resolution of confocal Raman, can probe core–shell compositional information using instrumentation and equipment accessible to nearly any laboratory or educational institution.

RESULTS AND DISCUSSION

Presented below is a method, similar to ice core analyses, for mapping solution composition as a function of depth using FTIR-ATR spectroscopy on small slices (6 mm diameter, ∼1–1.5 mm thick, 0.05–0.06 mL) of flash-frozen articulated (bendable) straws, which probes LLPS and related phase boundary conditions in aqueous solutions containing a salt and an organic species that mimic both brown carbon aerosol chemistry[26,26−31] and ATPE systems[23] along with analyzing intrasolution structural motifs that may be operative in core–shell particle morphologies. The solutions we use contain 3.0 M ammonium sulfate and 1.0 M concentration of one of eight alcohols (methanol, ethanol, 1-propanol, 2-propanol, 1,2-propanediol, 1,3-propanoediol, 2-butanol, and 3-methyl-2-butanol). The solutions are frozen and chopped into between 30 and 40 slices, depending on the alcohol, before analysis with

Received: July 27, 2021
Accepted: November 18, 2021
Published: November 30, 2021

https://doi.org/10.1021/acsomega.1c04014
ACS Omega 2021, 6, 33436–33442

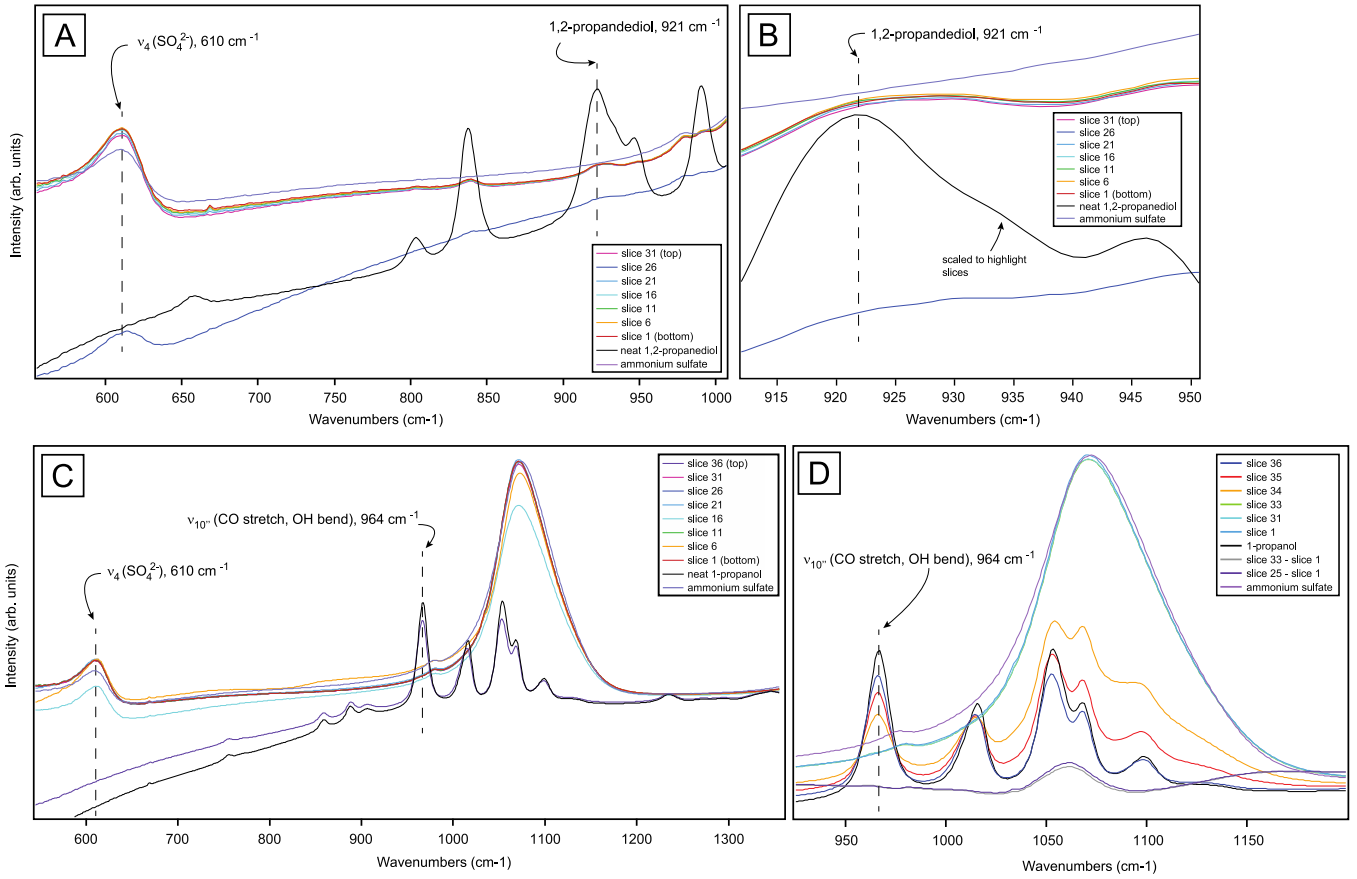

Figure 1. IR spectra for different depths in an articulated straw for 3.0 M ammonium sulfate solutions containing (a) 1.0 M 1,2-propanediol, (b) a close up of the 1,2-propanediol peak used for analysis, (c) 1.0 M 1-propanol, and (d) a close up of the 1-propanol peak used for analysis (slice 32 has been omitted due to an instrumental error). In each case, the spectra have been processed using a water background. Slices shown run from the bottom of the straw (slice 1) to the top (slice 31 of 33 for (a) and slice 36 of 36 for (c)). The sloped behavior is a consequence of background subtraction—layers with substantially less water content than the background appear with sloped intensity profiles.

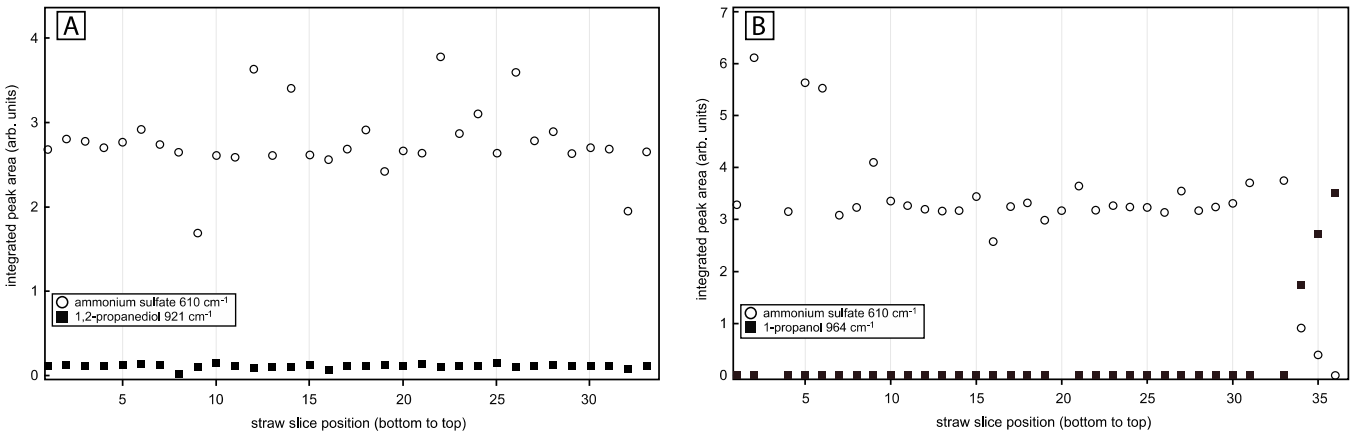

Figure 2. Integrated peak areas for solutions of an alcohol (1,2-propanediol (a) and 1-propanol (b)) and ammonium sulfate as a function of solution depth (with slice 1 corresponding to the bottom of the straw).

FTIR-ATR spectroscopy. Representative IR spectra for slices from two different solutions are shown in Figure 1. In panels A and B, the presence of alcohol IR peaks throughout the solution indicates that 1,2-propanediol is fully miscible and the solution lacks phase separation. However, spectra of the 1-propanol solution presented in panels C and D indicate the presence of LLPS. The separation can be seen in the differences between the topmost slices, with an alcohol peak (at 964 cm^{-1}) matching that from the neat alcohol and the lack of sulfate peaks at either 1074 or 610 cm^{-1}, and in the rest of the solution slices where no alcohol peaks exist. Thus, when LLPS forms in these systems, the organic phase sits exclusively at the top of the solution with the salty aqueous phase below.

An alternate way to visualize solution chemical composition versus depth is accomplished by comparing cleanly resolved spectral features for the alcohols and ammonium sulfate

https://doi.org/10.1021/acsomega.1c04014
ACS Omega 2021, 6, 33436−33442

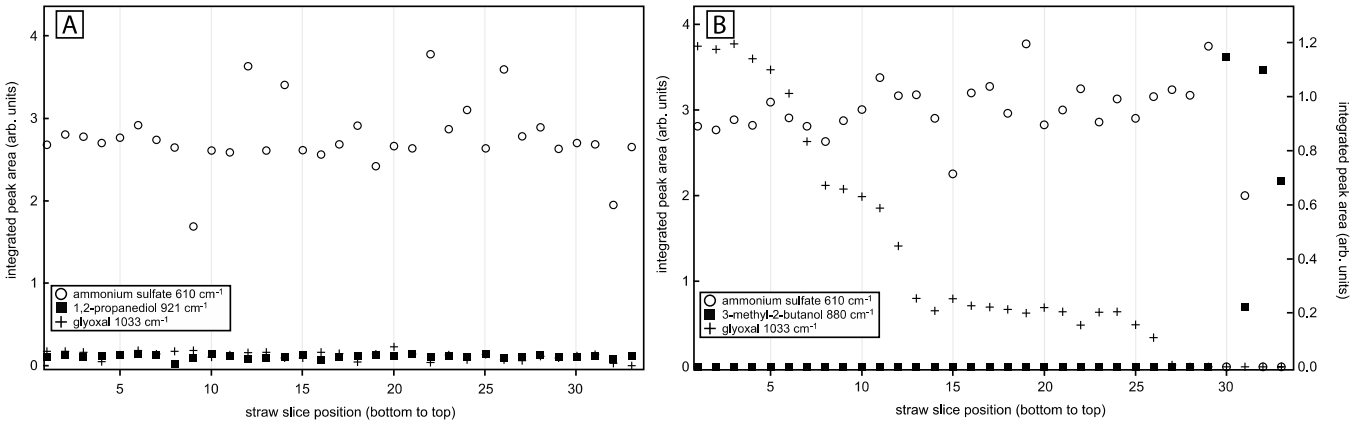

Figure 3. Integrated peak areas for solutions of an alcohol (1,2-propanediol (a) and 3-methyl-2-butanol (b)), ammonium sulfate, and glyoxal as a function of solution depth (with slice 1 corresponding to the bottom).

Table 1. Alcohol Physical Properties and Miscibility Results for 3.0 M Aqueous Ammonium Sulfate Solutions Containing 1.0 M Alcohol

alcohol	1,3-propanediol	1,2-propanediol	methanol	ethanol	2-propanol	1-propanol	2-butanol	3-methyl-2-butano
miscible? separable?	alcohol fully miscible				alcohol separates from the ammonium sulfate layer			
density (g/mL)	1.06	1.036	0.792s	0.789	0.786	0.803	0.806	0.818
$\log(K_{org/w})$	−1.04[a]	−0.92[a]	−0.74[b]	−0.30[b]	0.05[b]	0.25[b]	0.65[b]	1.28[b]
O/C ratio	0.667	0.667	1	0.5	0.333	0.333	0.25	0.2

[a]Ref 24. [b]Ref 25.

throughout a single solution. Figure 2 shows such a visualization (along with Figures S1−S5), with plots of the integrated peak areas of two cleanly resolved peaks for each slice from a frozen straw. We typically used the sulfate $\nu_4(SO_4^{2-})$ band, peaked here at 610 cm^{-1} with a FWHM of 30 cm^{-1},[32] and whichever alcohol peak was the most cleanly resolved in the fingerprint region. The qualitative results are robust and do not depend on the specific IR feature chosen for analysis (see Figure S1, both the $\nu_4(SO_4^{2-})$ peak at 610 cm^{-1} and the $\nu_4(NH_4^+)$ peak at 1440 cm^{-1} behave the same). The information extracted from the straw slices exposes an interesting feature of LLPS solutions because the small volumes and large number of slices allow us to probe the transition region between phases. The abrupt phase boundary can be seen in panel D of Figure 1 (slices 34−35), finishing completely within slice 34, as slice 33 shows no obvious alcohol IR peaks. Also shown in panel D of Figure 1 are differential comparisons between slice 1 (the bottom of the straw) and two intermediate slices, numbers 33 and 25 (all slices below 25 show identical behavior) that highlight the lack of a decreasing alcohol concentration as a function of distance from top of straw. A similar differential analysis (not shown) using the ammonium sulfate reference spectrum gives an identical result, showing that the alcohol can indeed be found only in the top fraction. An aqueous/organic transition region can be seen in the four other alcohols that exhibit LLPS (see Figures S2, S3, and 3). While the very top of the solution (the full organic phase, slice 36, Figure 1 panel D and Figure 2 panel B) appears to contain no ammonium sulfate, as observed in similar systems,[14] the transition layer carries information on the relationship between the two phases. There is no, for example, evidence of peak shifting in the transition region for either alcohol or sulfate, at least for these binary solutions, suggesting that the two species do not replace water interactions for sulfate−alcohol interactions (see Figure S6). Further work with higher resolution methods exploring this transition layer will be informative for understanding if, for example, the alcohol "pushes" the ammonium sulfate out of the way or out-competes it for water solvation.

Whether a solution will exhibit LLPS appears to depend on both the octanol−water partition coefficient (K_{OW}) and the O/C ratio. Of note, even though we find that the organic layer sits on top of the aqueous salt layer, this is not driven by density, as seen in Table 1, but rather it is likely due to the energy of interaction differences that favor alcohol−alcohol over alcohol−other interactions. Negative K_{OW} values correspond to a lack of LLPS, and positive K_{OW} values correspond to the presence of LLPS. The ability of the partition coefficient to predict LLPS formation is particularly relevant for systems containing molecules with no oxygen atoms (such as imidazole, as discussed later). While none of the solutions here contain an octanol phase, the hydrophobicity or hydrophilicity of the alcohol, indicated by the sign of K_{OW},[33,34] clearly relates to whether LLPS forms, and the extent of this predictability is an avenue of ongoing research. This LLPS dependence on the O/C ratio of the added organic species for ammonium sulfate/organic mixtures has been the subject of numerous studies.[9−12,15] These diverse experiments show that separation tends to occur for systems containing species with O/C ratios less than 0.44, never occurs for systems containing species with O/C ratios above 0.8, and is salt-dependent for intermediate O/C ratios. In broad agreement, we find that solutions with no LLPS have alcohol O/C ratios of 0.5 or larger, while solutions with LLPS have alcohol O/C ratios less than 0.5, as summarized in the table, and the capability of our solutions in frozen and sliced straws to recapture this known behavior is a useful test of the straw method.

https://doi.org/10.1021/acsomega.1c04014
ACS Omega 2021, 6, 33436−33442

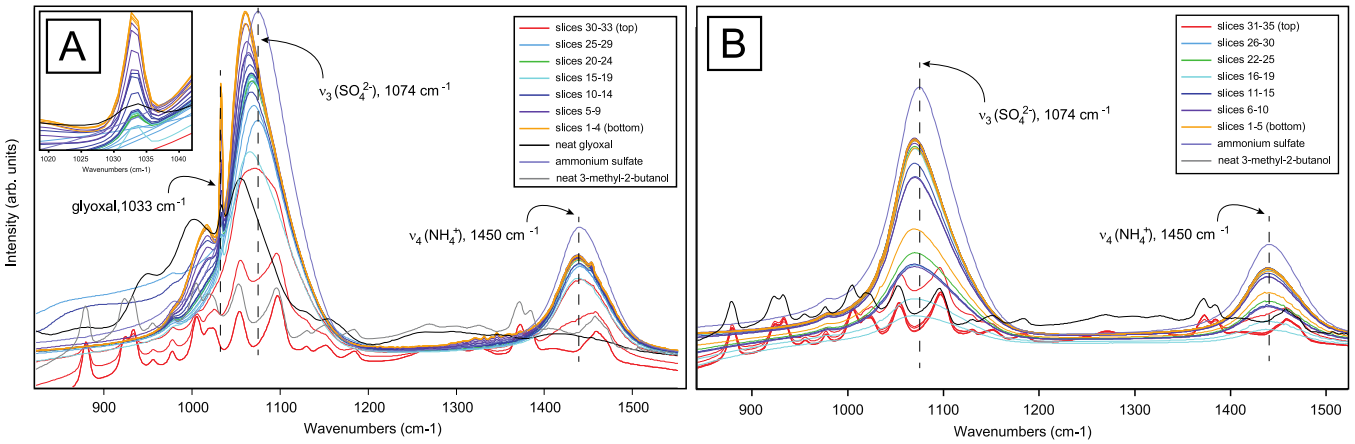

Figure 4. IR spectra for different depths in an articulated straw for 3.0 M ammonium sulfate solutions containing 3-methyl-2-butanol. The solution in panel A also contains 0.095 M glyoxal, while panel B does not. The inset of panel A shows a close up of the glyoxal peak used for analysis, at 1033 cm^{-1}.

A specific example of the usefulness of the sliced straw data, beyond merely identifying the presence or absence of LLPS, comes from how it may help explain our previous, bulk-phase kinetic data for aqueous ammonium sulfate solutions containing 3-methyl-2-butanol and glyoxal.[35] We posited that changes to the solvation environment upon addition of alcohol could create microregions of aggregated alcohol molecules in the bulk solution that excluded glyoxal and ammonium sulfate, the relevant reactants in the formation of imidazole-2-carboxaldehyde (IC) and biimidazole (BI), two components of brown carbon aerosol. In effect, these microregions would decrease the volume available to the reactants. The stratification data reported here cannot confirm or deny the presence of specific microheterogeneities themselves in the original solution, though they can tell when a glyoxal/ammonium sulfate/alcohol system exhibits LLPS and provide information on intrasolution interactions. As seen in Figure 3, if the alcohol forms no LLPS with ammonium sulfate (panel A, 1,2-propanediol); then, the glyoxal is fully miscible, but if the alcohol leads to LLPS formation (panel B, 3-methyl-2-butanol), the glyoxal stays in the ammonium sulfate layer.

The addition of glyoxal does not appear to alter whether or not LLPS forms, though it offers an important lesson for understanding more complicated solutions. Glyoxal miscibility follows ammonium sulfate—regardless of the alcohol—due to strong intermolecular interactions that depend appreciably on the sulfate concentration, and thus, miscibility should be insensitive to the alcohol.[36] The alcohol, and thus the presence or absence of LLPS can, however, still affect the glyoxal−sulfate interaction, as seen in the gradual decrease in glyoxal concentration in Figure 3 panel B, as a function of solution depth. A detailed view of this decrease can be seen in the spectra in Figure 4. When glyoxal is present in the 3-methyl-2-butanol and ammonium sulfate solution (panel A), there is a related peak shift for $\nu_3(SO_4^{2-})$ (centered at 1074 cm^{-1} in the reference spectrum). At the bottom of the straw, glyoxal is overrepresented and a complexation with the sulfate ion causes a shift in the sulfate peak. Just below the alcohol layer (slices 25−29 in panel A), there is less glyoxal present and the sulfate peak has shifted approximately 15 cm^{-1} to higher energy, to be in line with the reference position. The position of the $\nu_4(NH_4^+)$ peak, at 1450 cm^{-1}, does not shift, indicating no comparable glyoxal−ammonium interaction; the reaction partner for glyoxal is ammonia, not ammonium, so this lack of interactivity makes sense.[28,35,37] When no glyoxal is present, as seen in panel B, no sulfate peak shift is observed. Kurtén et al.[36] attribute the strength of the glyoxal−sulfate interaction to a "salting in" effect. When no LLPS forms, as in solutions with 1,2-propanediol (panel A of Figure 3), the glyoxal−sulfate interaction is broken up by the presence of alcohol throughout the solution (see Figure S6), and no sulfate peak shift occurs. Phase separation in the 3-methyl-2-butanol system excludes both glyoxal and ammonium sulfate from the topmost layers, resulting in an ammonium sulfate/glyoxal layer that is nearly 17% smaller in volume than if no alcohol was present. The increased reactant concentrations in this smaller volume increases the rate of product formation (for both IC and BI), even though the rate constants stay largely unchanged across the studied concentration range.[35]

Evidence of LLPS can inform our understanding of reactivity, though further work with glyoxal-containing solutions is needed. The same kinetic work[35] found that methanol and ethanol behave similarly to 3-methyl-2-butanol for IC production, with flat rate constants as a function of concentration. In contrast to 3-methyl-2-butanol, however, methanol and ethanol have concentration-dependent rate constants for BI formation. Both BI and imidazole—the first heterocycle formed—have negative octanol−water partition coefficients,[38] while IC has a positive K_{OW}.[39] Further work is needed to explore where these compounds sit within aged reaction solutions and whether new or additional layers form during aging. Characterizing how a solution changes internally as it ages will be useful for understanding the chemistry of formation of light-absorbing compounds in secondary organic aerosol mixtures containing oxidized hydrocarbons.

Despite the substantial size, volume, and surface area differences of these straw-based solutions versus atmospheric aerosol, and given previous observations consistent with the present work that find organics tend to partition to the outer layer while inorganics to the aqueous core,[9,11,19,40,41] reframing the tubes into the context of a sphere (see Figure S7) offers several useful insights. For example, a spherical particle of 50 nm radius with an alcohol layer representing 10% of the total volume (similar percentage to that observed in the straw data) can be calculated to have an outer layer of approximately 17 Å. This thickness corresponds to between 3 (for 3-methyl-2-

https://doi.org/10.1021/acsomega.1c04014
ACS Omega 2021, 6, 33436−33442

butanol) and 5 (for methanol) monolayers of alcohol at the surface of the particle, though this is best thought of as an upper bound for the shell thickness. Aerosol particles have a much larger surface area than a bulk solution confined to a straw, and given the volatility of the alcohols, evaporative losses (which we suppress in our bulk solutions, see below) that alter the size and composition of the organic layer are likely to occur. Assuming a core−shell morphology, reasonable given the substituents,[16] an outer organic layer is likely to affect a number of surface processes.[42,43] Isoprene epoxide (IEPOX) uptake into an aerosol was reduced in the presence of a particle with an organic coating,[43] surface tension was reduced for particles with organic surface coatings,[16] and bulk diffusion time scales increased with increasing phase separation.[42]

Another key variable that controls particle morphology and the formation and loss of LLPS in aerosol systems is the relative humidity (RH).[19,44,45] A mixed organic/inorganic particle, at high RH, is generally found to be homogeneous, transitioning to a phased system and different particle morphology states as the RH decreases. The bulk solution method reported here, as such, is not directly comparable with RH studies on single particles, at least in terms of measuring under what particle-scale conditions LLPS forms. Akin to the confocal Raman work of Wu et al. to map spectral differences between the core and shell of a drying droplet,[19] however, the work presented above is a window into the intrasolution interactions that may drive observed particle morphology and properties, for morphologies that exhibit similar solution stratification. The glyoxal concentration gradient seen in Figure 4, for example, suggests that under conditions when a particle exhibits a core−shell morphology, glyoxal is likely to be concentrated away from the outer organic layer, and this has direct implications on understanding intraparticle reactivity.

CONCLUSIONS

The straw technique presented here offers a robust way to probe for the presence of LLPS in aqueous organic−salt systems. By using aerosol- and separation science-relevant chemical mixtures, the method can be used to connect bulk-phase laboratory observations to particle-scale studies of similar systems and phenomena. In addition to the ability of this method to confirm known solution behavior—that LLPS forms when the O/C ratio of the organic component is approximately 0.5 or larger—the ability to freeze the solutions captures a moment in time. Taking this kind of a snapshot of a solution, for example as part of a kinetic experiment, can bring to light subtle differences in the way solution components organize themselves (such as the presence or absence of strong glyoxal−sulfate interactions along with LLPS), organization that can affect chemical reactivity, and also allows for studying the boundary region between phases in an LLPS system. Additional applications of this technique for visualizing intrasolution organization could include capturing ammonium sulfate salting out at high alcohol concentrations and analyzing the effect of alcohol (or other oxidized organic substituent) concentration on a system already exhibiting LLPS—relevant for ATPE work. In a nonaerosol application, this method could be an alternate way to build phase diagrams,[46] one that eliminates the perturbation introduced by sampling via syringes. These proposed uses should further our understanding of LLPS systems and the relationship between the chemical composition and solution structure within an aerosol particle.

EXPERIMENTAL METHODS

Glyoxal (Sigma Aldrich, 40% by weight in H_2O), ammonium sulfate (Sigma Aldrich, 99.0%), methanol (Pharmco-Aaper, 99.8%), ethanol (Pharmco-Aaper, 99.5%), 1-propanol (Sigma Aldrich, 99.5%), 2-propanol (Sigma Aldrich, 99.5%), 2-butanol (Sigma Aldrich, 99.5%), 3-methyl-2-butanol (Sigma Aldrich, 98%), 1,2-propanediol (Sigma Aldrich, 99.5%), and 1,3-propanediol (Sigma Aldrich, 98%) were used without further purification. All solutions were prepared in ultrapure water (18.2 MΩ, Thermo Scientific Barnstead NANOpure).

The articulated straw coring analysis method used above begins with preparation of the straws. The straws (6 mm diameter, 260 mm length, made of polypropylene, and purchased from Far East Brokers and Consultants) were first trimmed so that the end closest to the articulations was removed, resulting in the "bottom" end of the straw starting at the articulation section. This cut end was then wrapped with parafilm. After fully extending the articulated section of the straw, 2 mL of pre-prepared solution was added. Solution preparation is similar to that described elsewhere. Briefly, the solution contains 3.0 M ammonium sulfate and 1.0 M concentration of one of eight alcohols, mixed in ultrapure water. For solutions containing 0.095 M glyoxal, the glyoxal was added prior to the alcohol.

Once the solution was added to the straw, the loaded straw was tapped several times to release bubbles trapped in any of the articulations. Then, the portion of the straw containing liquid was fully submerged in a liquid nitrogen bath until frozen. We experimented with freezing speed and found that our results were repeatable only when the straws were directly and fully submerged. Slow freezing speeds, wherein the straw was incrementally submerged, allowed the solution to rearrange (on one occasion forcefully ejecting a portion out the top) or prevented freezing at all (liquid nitrogen temperatures were required, as solutions placed in a −80 °C freezer never solidified). Once frozen, the parafilm was removed and extra straw was removed from the top so that only the ice core portion remained.

The straws were sliced, using a razor blade, at each of the thinnest parts of the articulation to produce 30−40 slices (depending on the alcohol), each of approximately 2.5 mm thickness for a volume of 0.05−0.06 mL. Slices with smaller volumes or thicknesses are possible by using a different straw (smaller diameter, more closely spaced articulations), though we have not found any as yet. Each slice was placed into a 0.5 mL PCR tube immediately after being cut, and the razor blade wiped. The PCR tubes were placed on dry ice to prevent evaporative loss of alcohol and to prevent chemical reactivity in solutions containing both ammonium sulfate and glyoxal. If the frozen tube ever appeared to be melting, it was refrozen after resealing the bottom end with parafilm before slicing resumed. An example of the slicing process is shown in Figure 5.

After all slices had been transferred to PCR tubes, and stored on dry ice, they were taken for analysis using an FTIR-ATR instrument (Alpha Platinum, Bruker). Each sample (one slice stored in a PCR tube), now cold (but not frozen) and fully liquid, was placed under a cover slip on the ATR surface for analysis. This cover slip prevented evaporative alcohol loss during analysis and preserved chemical information without introducing new structural motifs (such as a droplet surface not present within the straw column). Infrared spectra were collected with 2 cm^{-1} resolution and averaged 60 times.

https://doi.org/10.1021/acsomega.1c04014
ACS Omega 2021, 6, 33436−33442

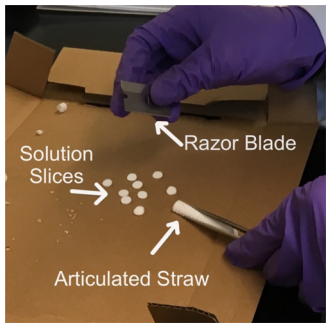

Figure 5. Example of slicing a frozen straw containing a 3.0 M ammonium sulfate and 1.0 M alcohol solution. To produce the data detailed in the main text, each slice was immediately moved to a PCR tube after being sliced.

Ultrapure water was used as a background. Peak analysis, to produce the data shown in the above figures, was done using the instrument's provided software (OPUS) by selecting a baseline around the peak of interest and integrating. Any postprocessing of the data was done using Igor Pro (version 6.37, WaveMetrics).

■ ASSOCIATED CONTENT

Supporting Information

The Supporting Information is available free of charge at https://pubs.acs.org/doi/10.1021/acsomega.1c04014.

Composition versus depth data for 1,3-propanediol, 2-butanol, 2-propanol, methanol, and ethanol; alternate sulfate peak integration data; and schematic of connection to particle-scale (PDF)

■ AUTHOR INFORMATION

Corresponding Author

Andrew E. Berke − *Department of Chemistry, Smith College, Northampton, Massachusetts 01063, United States;* orcid.org/0000-0001-7749-8079; Email: aberke@smith.edu

Authors

Emmaline R. Longnecker − *Department of Chemistry, Smith College, Northampton, Massachusetts 01063, United States*

Lucy Metz − *Department of Chemistry, Smith College, Northampton, Massachusetts 01063, United States*

Rebecca S. Miller − *Department of Chemistry, Smith College, Northampton, Massachusetts 01063, United States*

Complete contact information is available at: https://pubs.acs.org/10.1021/acsomega.1c04014

Notes

The authors declare no competing financial interest.

■ ACKNOWLEDGMENTS

We thank Dr. Charles Amass for help with the FTIR-ATR and Autumn Mineo for helpful conversations. We gratefully acknowledge funding from Smith College in support of this work.

■ REFERENCES

(1) Surratt, J. D.; Chan, A. W. H.; Eddingsaas, N. C.; Chan, M. N.; Loza, C. L.; Kwan, A. J.; Hersey, S. P.; Flagan, R. C.; Wennberg, P. O.; Seinfeld, J. H. Reactive Intermediates Revealed in Secondary Organic Aerosol Formation from Isoprene. *Proc. Natl. Acad. Sci. U. S. A.* **2010**, *107*, 6640−6645.

(2) Zuend, A.; Marcolli, C.; Peter, T.; Seinfeld, J. H. Computation of Liquid-Liquid Equilibria and Phase Stabilities: Implications for RH-Dependent Gas/Particle Partitioning of Organic-Inorganic Aerosols. *Atmos. Chem. Phys.* **2010**, *10*, 7795−7820.

(3) Zuend, A.; Seinfeld, J. H. Modeling the Gas-Particle Partitioning of Secondary Organic Aerosol: The Importance of Liquid-Liquid Phase Separation. *Atmos. Chem. Phys.* **2012**, *12*, 3857−3882.

(4) Song, Y. C.; Haddrell, A. E.; Bzdek, B. R.; Reid, J. P.; Bannan, T.; Topping, D. O.; Percival, C.; Cai, C. Measurements and Predictions of Binary Component Aerosol Particle Viscosity. *J. Phys. Chem. A* **2016**, *120*, 8123−8137.

(5) Bilde, M.; Svenningsson, B. CCN Activation of Slightly Soluble Organics: The Importance of Small Amounts of Inorganic Salt and Particle Phase. *Tellus B* **2004**, *56*, 128−134.

(6) Pósfai, M.; Buseck, P. R. Nature and Climate Effects of Individual Tropospheric Aerosol Particles. *Annu. Rev. Earth Planet. Sci.* **2010**, *38*, 17−43.

(7) Ott, E.-J. E.; Tackman, E. C.; Freedman, M. A. Effects of Sucrose on Phase Transitions of Organic/Inorganic Aerosols. *ACS Earth Space Chem.* **2020**, *4*, 591−601.

(8) Stewart, D. J.; Cai, C.; Nayler, J.; Preston, T. C.; Reid, J. P.; Krieger, U. K.; Marcolli, C.; Zhang, Y. H. Liquid-Liquid Phase Separation in Mixed Organic/Inorganic Single Aqueous Aerosol Droplets. *J. Phys. Chem. A* **2015**, *119*, 4177−4190.

(9) Song, M.; Ham, S.; Andrews, R. J.; You, Y.; Bertram, A. K. Liquid−Liquid Phase Separation in Organic Particles Containing One and Two Organic Species: Importance of the Average O : C. *Atmos. Chem. Phys.* **2018**, *18*, 12075−12084.

(10) Song, M.; Liu, P.; Martin, S. T.; Bertram, A. K. Liquid−Liquid Phase Separation in Particles Containing Secondary Organic Material Free of Inorganic Salts. *Atmos. Chem. Phys.* **2017**, *17*, 11261−11271.

(11) Song, M.; Marcolli, C.; Krieger, U. K.; Zuend, A.; Peter, T. Liquid-Liquid Phase Separation in Aerosol Particles: Dependence on O:C, Organic Functionalities, and Compositional Complexity. *Geophys. Res. Lett.* **2012**, *39*, 52807.

(12) You, Y.; Renbaum-Wolff, L.; Bertram, A. K. Liquid−Liquid Phase Separation in Particles Containing Organics Mixed with Ammonium Sulfate, Ammonium Bisulfate, Ammonium Nitrate or Sodium Chloride. *Atmos. Chem. Phys.* **2013**, *13*, 11723−11734.

(13) Ciobanu, V. G.; Marcolli, C.; Krieger, U. K.; Weers, U.; Peter, T. Liquid-Liquid Phase Separation in Mixed Organic/Inorganic Aerosol Particles. *J. Phys. Chem. A* **2009**, *113*, 10966−10978.

(14) Deming, B. L.; Ziemann, P. J. Measurements of the Partitioning of Nitric Acid and Sulfuric Acid in Aqueous/Organic Phase-Separated Systems. *Environ. Sci.: Atmos.* **2021**, 93.

(15) Song, Y.-C.; Bé, A. G.; Martin, S. T.; Geiger, F. M.; Bertram, A. K.; Thomson, R. J.; Song, M. Liquid−Liquid Phase Separation and Morphologies in Organic Particles Consisting of α-Pinene and β-Caryophyllene Ozonolysis Products and Mixtures with Commercially Available Organic Compounds. *Atmos. Chem. Phys.* **2020**, *20*, 11263−11273.

(16) Gorkowski, K.; Donahue, N. M.; Sullivan, R. C. Aerosol Optical Tweezers Constrain the Morphology Evolution of Liquid-Liquid Phase-Separated Atmospheric Particles. *Chem* **2020**, *6*, 204−220.

(17) Freedman, M. A. Liquid-Liquid Phase Separation in Supermicrometer and Submicrometer Aerosol Particles. *Acc. Chem. Res.* **2020**, *53*, 1102−1110.

(18) Craig, R. L.; Bondy, A. L.; Ault, A. P. Surface Enhanced Raman Spectroscopy Enables Observations of Previously Undetectable Secondary Organic Aerosol Components at the Individual Particle Level. *Anal. Chem.* **2015**, *87*, 7510−7514.

(19) Wu, F.-M.; Wang, X.-W.; Jing, B.; Zhang, Y.-H.; Ge, M.-F. Liquid-Liquid Phase Separation in Internally Mixed Magnesium Sulfate/Glutaric Acid Particles. *Atmos. Environ.* **2018**, *178*, 286−292.

(20) Zhou, Q.; Pang, S. F.; Wang, Y.; Ma, J. B.; Zhang, Y. H. Confocal Raman Studies of the Evolution of the Physical State of

Mixed Phthalic Acid/Ammonium Sulfate Aerosol Droplets and the Effect of Substrates. *J. Phys. Chem. B* **2014**, *118*, 6198−6205.
(21) Fu, H.; Dai, J.; Sun, Y.; Zhang, D.; Xiu, Z. Partition Behavior of Hydrophilic Diols in an Ethanol/Ammonium Sulfate Salting-out Extraction System. *Eng. Life Sci.* **2015**, *15*, 797−803.
(22) Guo, Y. X.; Han, J.; Zhang, D. Y.; Wang, L. H.; Zhou, L. L. An Ammonium Sulfate/Ethanol Aqueous Two-Phase System Combined with Ultrasonication for the Separation and Purification of Lithospermic Acid B from Salvia Miltiorrhiza Bunge. *Ultrason. Sonochem.* **2012**, *19*, 719−724.
(23) Wang, Y.; Yan, Y. S.; Hu, S. P.; Han, J.; Xu, X. H. Phase Diagrams of Ammonium Sulfate + Ethanol/1-Propanol/2-Propanol + Water Aqueous Two-Phase Systems at 298.15 K and Correlation. *J. Chem. Eng. Data* **2010**, *55*, 876−881.
(24) Krieger, U. K.; Marcolli, C.; Reid, J. P. Exploring the Complexity of Aerosol Particle Properties and Processes Using Single Particle Techniques. *Chem. Soc. Rev.* **2012**, *41*, 6631−6662.
(25) Song, M.; Marcolli, C.; Krieger, U. K.; Zuend, A.; Peter, T. Liquid-Liquid Phase Separation and Morphology of Internally Mixed Dicarboxylic Acids/Ammonium Sulfate/Water Particles. *Atmos. Chem. Phys.* **2012**, *12*, 2691−2712.
(26) Galloway, M. M.; Loza, C. L.; Chhabra, P. S.; Chan, A. W. H.; Yee, L. D.; Seinfeld, J. H.; Keutsch, F. N. Analysis of Photochemical and Dark Glyoxal Uptake: Implications for SOA Formation. *Geophys. Res. Lett.* **2011**, 38.
(27) Powelson, M. H.; Espelien, B. M.; Hawkins, L. N.; Galloway, M. M.; De Haan, D. O. Brown Carbon Formation by Aqueous-Phase Carbonyl Compound Reactions with Amines and Ammonium Sulfate. *Environ. Sci. Technol.* **2014**, *48*, 985−993.
(28) Yu, G.; Bayer, A. R.; Galloway, M. M.; Korshavn, K. J.; Fry, C. G.; Keutsch, F. N. Glyoxal in Aqueous Ammonium Sulfate Solutions: Products, Kinetics and Hydration Effects. *Environ. Sci. Technol.* **2011**, *45*, 6336−6342.
(29) De Haan, D. O.; Corrigan, A. L.; Smith, K. W.; Stroik, D. R.; Turley, J. J.; Lee, F. E.; Tolbert, M. A.; Jimenez, J. L.; Cordova, K. E.; Ferrell, G. R. Secondary Organic Aerosol-Forming Reactions of Glyoxal with Amino Acids. *Environ. Sci. Technol.* **2009**, *43*, 2818−2824.
(30) De Haan, D. O.; Corrigan, A. L.; Tolbert, M. A.; Jimenez, J. L.; Wood, S. E.; Turley, J. J. Secondary Organic Aerosol Formation by Self-Reactions of Methylglyoxal and Glyoxal in Evaporating Droplets. *Environ. Sci. Technol.* **2009**, *43*, 8184−8190.
(31) De Haan, D. O.; Hawkins, L. N.; Kononenko, J. A.; Turley, J. J.; Corrigan, A. L.; Tolbert, M. A.; Jimenez, J. L. Formation of Nitrogen-Containing Oligomers by Methylglyoxal and Amines in Simulated Evaporating Cloud Droplets. *Environ. Sci. Technol.* **2011**, *45*, 984−991.
(32) Weis, D. D.; Ewing, G. E. Infrared Spectroscopic Signatures of (NH4)2SO4 Aerosols. *J. Geophys. Res.: Atmos.* **1996**, *101*, 18709−18720.
(33) Meylan, W.; Howard, P. Atom Fragment Contribution Method for Estimating Octanol-Water Partition-Coefficients. *J. Pharm. Sci.* **1995**, *84*, 83−92.
(34) *Exploring QSAR: Hydrophobic, Electronic, and Steric Constants*; Hansch, C., Leo, A., Hoekman, D., Eds.; ACS Professional Reference Book; American Chemical Society: Washington, DC, 1995; Vol. *2*.
(35) Berke, A. E.; Bhat, T. A.; Myers, H.; Gubbins, E. F.; Nwankwo, A. A. O.; Lu, K.; Timpane, L.; Keller, C. Effect of Short-Chain Alcohols on the Bulk-Phase Reaction between Glyoxal and Ammonium Sulfate. *Atmos. Environ.* **2019**, *198*, 407−416.
(36) Kurtén, T.; Elm, J.; Prisle, N. L.; Mikkelsen, K. V.; Kampf, C. J.; Waxman, E. M.; Volkamer, R. Computational Study of the Effect of Glyoxal−Sulfate Clustering on the Henry's Law Coefficient of Glyoxal. *J. Phys. Chem. A* **2015**, *119*, 4509−4514.
(37) Noziere, B.; Dziedzic, P.; Cordova, A. Products and Kinetics of the Liquid-Phase Reaction of Glyoxal Catalyzed by Ammonium Ions (NH4+). *J. Phys. Chem. A* **2009**, *113*, 231−237.
(38) Kim, S.; Chen, J.; Cheng, T.; Gindulyte, A.; He, J.; He, S.; Li, Q.; Shoemaker, B. A.; Thiessen, P. A.; Yu, B.; Zaslavsky, L.; Zhang, J.; Bolton, E. E. PubChem in 2021: New Data Content and Improved Web Interfaces. *Nucleic Acids Res.* **2021**, *49*, D1388−D1395.
(39) Wildman, S. A.; Crippen, G. M. Prediction of Physicochemical Parameters by Atomic Contributions. *J. Chem. Inf. Comput. Sci.* **1999**, *39*, 868−873.
(40) Song, M.; Marcolli, C.; Krieger, U. K.; Lienhard, D. M.; Peter, T. Morphologies of Mixed Organic/Inorganic/Aqueous Aerosol Droplets. *Faraday Discuss.* **2013**, *165*, 289−316.
(41) You, Y.; Smith, M. L.; Song, M.; Martin, S. T.; Bertram, A. K. Liquid-Liquid Phase Separation in Atmospherically Relevant Particles Consisting of Organic Species and Inorganic Salts. *Int. Rev. Phys. Chem.* **2014**, *33*, 43−77.
(42) Slade, J. H.; Ault, A. P.; Bui, A. T.; Ditto, J. C.; Lei, Z. Y.; Bondy, A. L.; Olson, N. E.; Cook, R. D.; Desrochers, S. J.; Harvey, R. M.; Erickson, M. H.; Wallace, H. W.; Alvarez, S. L.; Flynn, J. H.; Boor, B. E.; Petrucci, G. A.; Gentner, D. R.; Griffin, R. J.; Shepson, P. B. Bouncier Particles at Night: Biogenic Secondary Organic Aerosol Chemistry and Sulfate Drive Diel Variations in the Aerosol Phase in a Mixed Forest. *Environ. Sci. Technol.* **2019**, *53*, 4977−4987.
(43) Zhang, Y.; Chen, Y.; Lambe, A. T.; Olson, N. E.; Lei, Z.; Craig, R. L.; Zhang, Z.; Gold, A.; Onasch, T. B.; Jayne, J. T.; Worsnop, D. R.; Gaston, C. J.; Thornton, J. A.; Vizuete, W.; Ault, A. P.; Surratt, J. D. Effect of the Aerosol-Phase State on Secondary Organic Aerosol Formation from the Reactive Uptake of Isoprene-Derived Epoxydiols (IEPOX). *Environ. Sci. Technol. Lett.* **2018**, *5*, 167−174.
(44) Kucinski, T. M.; Ott, E.-J. E.; Freedman, M. A. Flash Freeze Flow Tube to Vitrify Aerosol Particles at Fixed Relative Humidity Values. *Anal. Chem.* **2020**, *92*, 5207−5213.
(45) Kucinski, T. M.; Ott, E.-J. E.; Freedman, M. A. Dynamics of Liquid−Liquid Phase Separation in Submicrometer Aerosol. *J. Phys. Chem. A* **2021**, *125*, 4446−4453.
(46) Feng, Z. Y.; Li, J. Q.; Sun, X. T.; Sun, L. Y.; Chen, J. Q. Liquid-Liquid Equilibria of Aqueous Systems Containing Alcohol and Ammonium Sulfate. *Fluid Phase Equilib.* **2012**, *317*, 1−8.

https://doi.org/10.1021/acsomega.1c04014
ACS Omega 2021, 6, 33436−33442